Electrohydrodynamic instability in an annular liquid layer with radial conductivity gradients

Zijing Ding* and Teck Neng Wong†
School of Mechanical and Aerospace Engineering, Nanyang Technological University, Singapore, 639798
(Received 13 December 2013; published 12 March 2014)

In this paper, the electrohydrodynamic stability in an annular liquid layer with a radial electrical conductivity gradient is investigated. A weak shear flow arises from a constant pressure gradient in the axial direction. In the radial direction, an electric field is applied. The three-dimensional linear instability analysis is implemented to study the influence of the inner radius, electrical conductivity gradient, shear flow, and ionic diffusion on the dynamics of the fluid layer. It is found that the critical unstable mode may either be oscillatory or stationary. The system becomes more unstable as the dimensionless inner radius a increases. When the inner radius a is small, the critical unstable mode is stationary, while it is given by three-dimensional oblique waves when a is large. When the conductivity gradient is small, the critical unstable mode is the three-dimensional oblique wave, while when the conductivity gradient is large, it would switch to the stationary mode rather than the oscillatory mode. The system becomes more unstable when the Reynolds number is slightly increased from zero. Additionally, it is found that the electrical Schmidt number has dual effects. The liquid layer becomes either more unstable or stable as the electric Schmidt number increases.

DOI: 10.1103/PhysRevE.89.033010 PACS number(s): 47.20.−k, 47.65.−d

I. INTRODUCTION

Electrohydrodynamics has attracted much attention since the last century due to its widely promising applications in microfluidic devices, such as in ink-jet printers [1] and in drug delivery [2]. In microscale flows, the flow is laminar and mixing due to turbulence will not occur. The use of an electric field is a potential approach to enhance the mixing in microfludic devices which has received many investigations [3]. When an external electric field is applied across a liquid layer, the Maxwell stress is imposed upon the liquids. The Maxwell stress could initiate flow instability in the liquid layer with spatial changes in electrical properties. In previous studies, the instability of flow systems may be triggered by an electric field due to abrupt changes in the electrical properties [4–8] or spatial gradients in electrical properties [9–11].

The former study of abrupt changes in electrical properties across the liquid layers investigates the influence of Maxwell stress on the interfacial instability. It is assumed that there is no electrical charge within the bulk region, while electrical charges accumulate on the interface. Such a model proposed was the leaky-dielectric model by Taylor [12]. Burcham and Saville [13] investigated the instability of a liquid bridge in the presence of an external electric field. They indicated that the Rayleigh-Plateau instability can be suppressed if the electrical conductivity of the bridge was larger than the conductivity of its surrounding gas. López-Herrera *et al*. [14] discussed the influence of surrounding gases on the instability of liquid jets in an external radial electric field. They dropped the assumption of perfect conducting liquids, but considered finite electrical conductivity and permittivity to describe a situation increasingly prevalent in the sector of small-scale free-surface flows [14]. Wang [15] discussed the influence of surface charge transportation on the breakup of a poorly conducting liquid thread in a radial electric field. Ding *et al*. investigated the instability of pressure-driven coflows in an annulus duct in a radial electric field [16]. The liquids were considered to be leaky dielectrics, and there was an abrupt change in the electrical conductivity as well as the electrical permittivity. Their results showed that the electric field can either enhance or impede the capillary instability caused by surface tension and interfacial wave instability due to viscosity stratification [16]. Recently Wray *et al*. [17,18] used the radial electric field to control the interfacial instability in an annular liquid film flowing down a vertical cylinder.

The latter study of liquids with spatial electrical conductivity gradients focused on the influence of an electrical body force on the electroconvection. The electrical body force may be exerted by imposing an external electric field or a self-induced electric field of free ions in the liquid. In microfluidics, the application of electrohydrodynamic mixing is based on gradients of electrical conductivity because the mechanical techniques are not suited to obtaining mixing for the requirement of prohibitive amounts of power [19]. The electrical conductivity can be developed due to a superimposed electrical field [20]. Baygents and Baldessari investigated the instability of a liquid layer with a wall-normal conductivity gradient between two parallel planar plates [21]. In Ref. [21] it was indicated that the local ionic concentration, pH value, and conductivity gradients developed along the axis of the imposed electric field and the local conductivity could vary by more than an order of magnitude over a length of 1 mm. Baygents and Baldessari proposed that the occurrence of instability was triggered by the dielectrophoretic effect [21]. They found that the lower conductivity boundary had a strong stabilizing effect when the conductivity gradient was large [21]. It should be noted that the assumption of exchange of stability made by Baygents and Baldessari [21] was incorrect because the critical unstable mode may be oscillatory as pointed out by Chang *et al*. [22]. While the instability mechanism can be analog to the classical Rayleigh-Bénard instability in a heated fluid layer, the physical mechanism is much more complex. For instance, in a single heated fluid layer where one imposes a shear flow, the critical unstable mode is always dominated by the longitudinal

*zding001@e.ntu.edu.sg
†mtnwong@ntu.edu.sg

mode, which is independent of the shear flow [23,24], while the critical unstable mode in the liquid layer with an electrical conductivity gradient depends on the shear flow heavily. Chang *et al*. [22] found that when the Reynolds number was slightly increased from zero, the instability was enhanced since the shear flow enhanced the dielectrophoretic effect and the transverse mode (zero spanwise wave number) became critical rather than the longitudinal model (zero streamwise wave number). However, as the Reynolds number was increased further, they found that the longitudinal mode became critical, and the critical mode was independent of the shear flow. Chang *et al*. [22] reported in their paper that the critical unstable mode was oscillatory when the conductivity gradient was small, but it switched to the stationary mode as the conductivity gradient increased. Ruo *et al*. [25] extended the model [22] by considering the rotating effect, but without imposing a shearing flow. Their results demonstrated that rotation played a stabilizing role in the system [25]. In Refs. [21,22,25], the instabilities are triggered by an external electric field. When the electric field is induced by free ions, the electric field may also initiate flow instability. The instability of such flows in a circular pipe has been investigated by Georgiou *et al*. [26] and extended by Conroy and his coworkers [27–29].

The electrical body force can also be induced by the nonisothermal effect even if there are no free charges in the system. Shivakumaraa *et al*. [30] investigated the Rayleigh-Bénard instability of a rotating liquid layer in an ac electric field. Shivakumaraa *et al*. [30] considered that the conductivity and permittivity gradients were induced by a temperature gradient which was imposed between the two parallel plates. Nevertheless, Shivakumaraa *et al*. [30] simplified the problem to an electrostatic problem by assuming that the frequency of the electric field was very high. They found that rotation impeded the heat convection while the electric field enhanced the heat convection. Recently Yoshikawa *et al*. investigated a dielectrophoretic Rayleigh-Bénard convection in a plane channel in a microgravity environment via a direct simulation and linear stability analysis [31]. In annulus ducts, the thermal convection instabilities coupled with an electric field were studied through considering that the electrical properties were dependent of local temperature [32–34]. The electric field was found to enhance the heat convection, thus destabilizing the system. Such a method can be used to enhance mixing in macroscale flows [30–34]. However, very few studies were made on the three-dimensional convection instability due to the electrical conductivity gradient subject to a shear flow in the annulus duct in anisothermal system. In such an annulus system, the radius ratio between the inner cylinder and the outer cylinder will play an important role in determining the critical unstable mode since the velocity profile, the distribution of the charge density, and the electric field depend on the radius ratio heavily, which motivates us to carry out the study of this system.

The rest of this paper is organized as follows. In Sec. II the mathematical formulation is constructed. Section III presents the base state and nondimensional governing system. In Sec. IV the linear stability analysis is implemented and the normal mode analysis is considered. In the first part of Sec. V, we first validate our numerical method by reducing the annular system to a planar system and compare our results with that of Chang *et al*. [22]; the second part of Sec. V discusses the influence of the inner radius, the conductivity gradient, the Reynolds number, and the electrical Schmidt number on the stability of the liquid layer. In the last section, a conclusion is made.

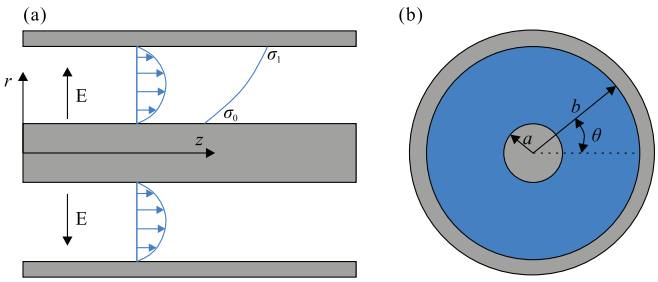

FIG. 1. (Color online) Geometry of the system. (a) Side view. (b) Cross-view.

II. MATHEMATICAL FORMULATION

We consider an annulus system as shown in Fig. 1. The liquids are eletrolyte solutions and considered to be Newtonian with constant density ρ, kinematical viscosity ν, and dynamical viscosity $\mu = \rho\nu$. An electric field is imposed in the radial direction, and a constant pressure gradient is imposed along the axis.

In this paper the three-dimensional hydrodynamical problem is considered. The cylindrical coordinates (r,θ,z) are chosen. Gravity is neglected. Fluids are governed by the continuity equation and the momentum equation,

$$\nabla \cdot \mathbf{v} = 0, \tag{1}$$

$$\rho \frac{D\mathbf{v}}{Dt} = -\nabla p + \mu \nabla^2 \mathbf{v} + \mathbf{f}, \tag{2}$$

where $\mathbf{v} = u\mathbf{e}_r + v\mathbf{e}_\theta + w\mathbf{e}_z$ is the velocity. $\frac{D}{Dt}$ is the material derivative operator. $\mathbf{f}$ is the electrical force, which can be related to the Maxwell stress tensor $\mathbb{T}^M$ by

$$\mathbf{f} = \nabla \cdot \mathbb{T}^M. \tag{3}$$

Usually analysis of Eq. (2) is difficult because the electric field is coupled to the free charge density ρ_e according to Maxwell's equations. Moreover, the free charge density is coupled to the flow field. In this paper we assume that the electrical current density $\mathbf{J}_e$ as well as the induced current density $\frac{\partial \epsilon \mathbf{E}}{\partial t}$ are modest so that the induced magnetic field is negligible. Therefore, the electrostatic problem is considered in this paper:

$$\nabla \times \mathbf{E} = 0. \tag{4}$$

Hence, the Maxwell stress $\mathbb{T}^M = \epsilon \mathbf{E}\mathbf{E} - \frac{1}{2}\epsilon \|\mathbf{E}\|^2 \mathbb{I}$. The parameter ϵ is the dielectric permittivity and $\mathbf{E}$ is the electric field. Here $\|\mathbf{E}\|^2 = \mathbf{E} \cdot \mathbf{E}$ and $\mathbb{I}$ is the identity tensor. Since the charge density is given by Gauss's law,

$$\rho_e = \nabla \cdot (\epsilon \mathbf{E}), \tag{5}$$

the momentum equation (2), now is rewritten as

$$\rho \frac{D\mathbf{v}}{Dt} = -\nabla p + \mu \nabla^2 \mathbf{v} + \rho_e \mathbf{E} - \frac{1}{2}\|\mathbf{E}\|^2 \nabla \epsilon. \tag{6}$$

The term $\frac{1}{2}\|\mathbf{E}\|^2\nabla\epsilon$ is ignored in this paper, and the electrical permittivity ϵ is assumed to be constant.

Since we are considering the electrostatics, the electric field $\mathbf{E}$ can be related to the gradient of electrical potential by

$$\mathbf{E} = -\nabla\phi. \tag{7}$$

Conservation of electrical charge gives

$$\frac{\partial\rho_e}{\partial t} + \nabla\cdot\mathbf{J}_e = 0. \tag{8}$$

In this paper we consider the liquid as an Ohmic conductor which neglects the diffusion of the charge; then the current density $\mathbf{J}_e$ is given by

$$\mathbf{J}_e = \sigma\mathbf{E} + \rho_e\mathbf{v}, \tag{9}$$

where σ is the electrical conductivity. Substituting Eq. (9) into the current conservative law, we obtain

$$\frac{D\rho_e}{Dt} + \nabla\cdot(\sigma\mathbf{E}) = 0. \tag{10}$$

Since we are considering an ionic conductor, the conductivity of which is dependent on the local ionic concentration, the conductivity can be described by the following diffusion equation as proposed by Melcher [35]:

$$\frac{D\sigma}{Dt} = K_{\text{eff}}\nabla^2\sigma, \tag{11}$$

where K_{eff} is an effective diffusivity due to the Brownian motion of the ions [21,22]. Lin *et al.* derived a similar equation describing the diffusion of electrical conductivity from the species conservation law [9], and the electrical conductivity was linearly dependent on the ionic concentration. The effective diffusivity K_{eff} can be related to the diffusive coefficients of species in the work of Lin *et al.* through a linear combination [9]. Equation (11) is valid if the local electrical time is much faster than the fluid time and the time for ion electromigration [21,22],

$$\frac{\epsilon}{\sigma_0} \ll \frac{d}{\Omega E_0} \ll \frac{d^2}{\nu} \quad\text{and}\quad \frac{d^2}{\Omega k_B T}, \tag{12}$$

in which $k_B T$ is the Boltzmann temperature, Ω is a characteristic mobility of the charge-carrying solutes, and d is the thickness of the liquid. The diffusive term $K_{\text{eff}}\nabla^2\sigma$ was suggested by Baygents and Baldessari [21], who indicated that the diffusion term had a stabilizing effect and was responsible for the existence of a threshold electric field, below which the flow was stable. This was also pointed out in Ref. [9]. In Ref. [22], it is implied that when the diffusion term is neglected, the transverse mode is always stable. In addition, the diffusion is responsible for the conductivity profile at the steady state [19]. Hence, in this paper the diffusion term should be retained, and its effect on the stability of the flow will be discussed.

At the inner boundary $r = a$, there are nonslip and nonpenetration boundary conditions:

$$u = v = w = 0. \tag{13}$$

The electrical conductivity at $r = a$ is given as

$$\sigma = \sigma_0. \tag{14}$$

At the outer boundary, $r = b$, the nonslip and nonpenetration conditions are considered:

$$u = v = w = 0. \tag{15}$$

The electrical conductivity at $r = b$ is given as well:

$$\sigma = \sigma_1. \tag{16}$$

III. NONDIMENSIONALIZATION AND BASE STATE

A. Dimensional base state

The velocity in the radial and azimuthal directions vanishes at the base state, i.e., $\bar{u} = \bar{v} = 0$. The flow is parallel to the axis, which is driven by a constant pressure gradient $\frac{\partial\bar{p}}{\partial z} = C$. The electric field is parallel to the radial direction at the base state. Therefore, the flow field and the electric field are decoupled. The velocity profile at the base state is

$$\bar{w} = \frac{C}{4\mu}\left[r^2 - \frac{b^2\ln(r/a) - a^2\ln(r/b)}{\ln(b/a)}\right]. \tag{17}$$

The pressure $\bar{p}$ at the base state is written as $\bar{p} = f(r) + Cz$. The variables with the over bars represent the respective variables at the base state.

Assuming that the shear flow does not disturb the steady conductivity profile, then the conductivity profile at the base state is described by

$$\bar{\sigma} = \frac{\sigma_1\ln(r/a) - \sigma_0\ln(r/b)}{\ln(b/a)}. \tag{18}$$

The electric field is obtained from the charge conservation equation (10),

$$\bar{E}_r = \frac{aE_0\sigma_0\ln(b/a)}{r[\sigma_1\ln(r/a) - \sigma_0\ln(r/b)]}, \tag{19}$$

where E_0 is the electric strength at $r = r_0$. We notice that the per unit length current $\mathbf{i}$ across the fluid layer (the length is along the axial direction) can be defined as $\mathbf{i} = \mathbf{e}_r\int_0^{2\pi}\bar{\sigma}\bar{E}_r r\,d\theta$. At the base state, $\mathbf{i} = a\sigma_0 E_0\mathbf{e}_r$ is constant, indicating that a constant electrical current is applied across the fluid layer. The electric strength at $r = b$ is $E_r = \frac{a\sigma_0}{b\sigma_1}E_0$.

The electrical potential at the base state is defined as

$$\bar{\phi} = \phi_0 - aE_0\sigma_0\ln(b/a)\frac{\ln[\sigma_1\ln(r/a) - \sigma_0\ln(r/b)]}{\sigma_1 - \sigma_0}, \tag{20}$$

where ϕ_0 is the reference electrical potential.

The charge density $\bar{\rho}_e$ is obtained from Gauss's law:

$$\bar{\rho}_e = \epsilon\left(\frac{1}{r}\frac{\partial rE_r}{\partial r}\right) = -\frac{\epsilon(\sigma_1 - \sigma_0)aE_0\sigma_0\ln(b/a)}{r^2[\sigma_1\ln(r/a) - \sigma_0\ln(r/b)]^2}. \tag{21}$$

B. Nondimensional system

We introduce the nondimensional scales: the length scale $d = b - a$, the velocity scale $W = -\frac{Cd^2}{8\mu}$, the time scale d/W, the pressure scale ρW^2, the electric strength scale E_0, the conductivity scale $\Delta\sigma = \sigma_1 - \sigma_0$, and the charge density scale $\epsilon\frac{E_0\Delta\sigma}{d\sigma_0}$. The current density $\mathbf{J}_e$ is scaled by referring to $E_0\sigma_0$, and the nondimensional $\mathbf{J}'_e$ is expressed as

$$\mathbf{J}'_e = \frac{\Delta\sigma}{\sigma_0}\sigma'\mathbf{E}' + \mathbf{E}' + \frac{\Delta\sigma}{\sigma_0}\frac{\epsilon/\sigma_0}{d/W}\rho'_e\mathbf{v}'. \tag{22}$$

Naturally the dimensionless governing equations emerge:

$$\nabla \cdot \mathbf{v} = 0, \tag{23}$$

$$\frac{D\mathbf{v}}{Dt} = -\nabla p + \frac{1}{\mathrm{Re}}\nabla^2 \mathbf{v} + Q\nabla^2\phi\nabla\phi, \tag{24}$$

$$\frac{D(\nabla^2\phi)}{Dt} + R_t[(1+\eta\sigma)\nabla^2\phi + \eta\nabla\phi\cdot\nabla\sigma] = 0, \tag{25}$$

$$\frac{D\sigma}{Dt} = \frac{1}{\mathrm{ReSc}_e}\nabla^2\sigma, \tag{26}$$

where the electrical charge ρ_e in the momentum equation is eliminated by using the dimensionless Poisson's equation,

$$\rho_e = -\frac{1}{\eta}\nabla^2\phi. \tag{27}$$

$\mathrm{Re} = \frac{Wd}{\nu}$ is the Reynolds number; $Q = \frac{\epsilon E_0^2}{\rho W^2}$ measures the ratio of electrical force to inertia force; $\eta = \frac{\Delta\sigma}{\sigma_0}$; $R_t = \frac{d/W}{\epsilon/\sigma_0}$ measures the ratio of viscous time to electrical time; and $\mathrm{Sc}_e = \frac{\nu}{K_{\mathrm{eff}}}$ is the Schmidt number. The parameter $R_t = \frac{1}{\mathrm{Re}}\frac{d^2\sigma_0}{\nu\epsilon}$ is usually a large number and has a magnitude of 10^7 provided that $\mathrm{Re} = O(1)$, $d = 10^{-3}\mathrm{m}$, $\sigma_0 = 10^{-2}\mathrm{S/m}$, $\epsilon = 10^{-9}\mathrm{C/(m\cdot V)}$, and $\nu = 10^{-6}\mathrm{m^2/s}$. Hence, the term $\frac{D(\nabla^2\phi)}{Dt}$ in Eq. (25) can be neglected [22].

The dimensionless boundary conditions at $r = a$ are

$$u = v = w = 0, \tag{28}$$

$$\sigma = 0. \tag{29}$$

At $r = b$, the dimensionless boundary conditions can be written as

$$u = v = w = 0, \tag{30}$$

$$\sigma = 1. \tag{31}$$

The dimensionless base state is defined as

$$\bar{w} = -2\left[r^2 - \frac{(b^2-a^2)\ln(r/a) + a^2\ln(b/a)}{\ln(b/a)}\right], \tag{32}$$

$$\bar{\sigma} = \frac{\ln(r/a)}{\ln(b/a)}, \tag{33}$$

$$\bar{E}_r = \frac{a\ln(b/a)}{r[\eta\ln(r/a) + \ln(b/a)]}, \tag{34}$$

$$\bar{\phi} = -\frac{a\ln(b/a)}{\eta}\ln[\eta\ln(r/a) + \ln(b/a)], \tag{35}$$

$$\bar{\rho}_e = -\frac{a\ln(b/a)}{r^2[\eta\ln(r/a) + \ln(b/a)]^2}. \tag{36}$$

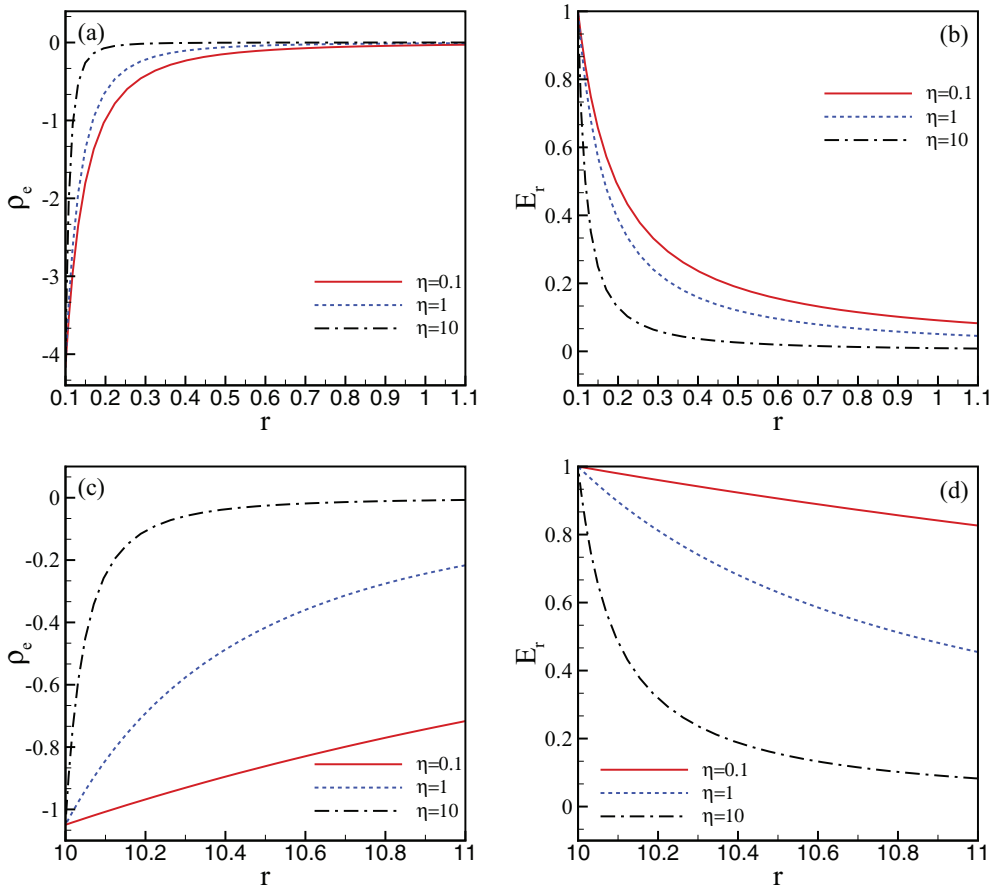

FIG. 2. (Color online) (a), (c) Charge density of the base state. (b), (d) Strength of the electric field at the base state. (a) and (b) are plotted at the dimensionless radius $a = 0.1$; (c) and (d) are plotted at the dimensionless radius $a = 10$.

Note that the charge density $\bar{\rho}_e$ is negative, while the base state of the electric field is positive. Therefore, the electrical body force $\rho_e \mathbf{E}$ acts in the opposite direction to the radial direction. The base state (32)–(36) of this system depends on the inner radius a and the electrical conductivity gradient η. The charge density $\bar{\rho}_e$ and electric-field strength $\bar{E}_r$ are plotted in Fig. 2. Comparing Figs. 2(b) with 2(d), it is observed that, the electric-field strength decreases more rapidly for a smaller a. For instance, when $a = 0.1$, $\eta = 10$, E_r decreases from 1 to 0.1 near $r = 0.3$. However, when $a = 10$, $\eta = 10$, the electric-field strength E_r decreases from 1 to 0.1 near $r = 10.8$. The charge density also decreases more rapidly for a smaller a by comparing Figs. 2(a) with 2(c). Furthermore, in Fig. 2, it implies that, for a large conductivity gradient η, the portion of the fluid layer where the electrical force $\bar{\rho}_e \bar{E}_r$ is appreciable is proximal to the inner surface.

IV. LINEAR STABILITY ANALYSIS

Although we have obtained the base state analytically in Sec. III, it is not necessary to be stable. To investigate the stability of the flow, we apply the linear stability theory by introducing infinitesimal disturbances into the system:

$$\mathbf{v} = \bar{\mathbf{v}} + \mathbf{v}', \quad p = \bar{p} + p', \quad \phi = \bar{\phi} + \phi', \quad \sigma = \bar{\sigma} + \sigma'. \tag{37}$$

The variables $\mathbf{v}' = u'\mathbf{e}_r + v'\mathbf{e}_\theta + w'\mathbf{e}_z$, p', ϕ', and σ' are the infinitesimal disturbances. Substituting the perturbed variables $(\mathbf{v}, p, \phi, \sigma)$ into the dimensionless governing equations, and after linearizing, we obtain the governing equations of the infinitesimal disturbances, which are shown in the Appendix, Eqs. (A1)–(A6).

In a standard way, we consider the normal mode analysis,

$$\begin{pmatrix} \mathbf{v}' \\ p' \\ \phi' \\ \sigma' \end{pmatrix} = \begin{pmatrix} \hat{\mathbf{v}}(r) \\ \hat{p}(r) \\ \hat{\phi}(r) \\ \hat{\sigma}(r) \end{pmatrix} \exp[i(n\theta + kz) + \lambda t], \tag{38}$$

where k is the streamwise wave number, n is the azimuthal wave number, $\lambda = \lambda_r + i\lambda_i$ is the complex temporal growth rate whose real part λ_r describes the exponential growth rate of the amplitudes of disturbances, and the "hats" denote the Fourier amplitudes of disturbances. The normal mode analysis results in the eigenvalue problem of λ.

The velocity and electrical conductivity at $r = a, b$ are fixed, and thus boundary conditions of the perturbed system at $r = a, b$ are expressed as follows:

$$\hat{u} = \hat{v} = \hat{w} = \hat{\sigma} = 0. \tag{39}$$

We assume that the radial component of the electric field E_r at the boundary is fixed; then the perturbed conditions of electric potential at the inner and outer surface are

$$\frac{d\hat{\phi}}{dr} = 0. \tag{40}$$

A Chebyshev collocation method is implemented to resolve the eigenvalue problem, and the physical domain is transformed to the Chebyshev domain:

$$\zeta = 2\frac{r-a}{b-a} - 1. \tag{41}$$

The variables $\hat{u}$, $\hat{v}$, $\hat{w}$, $\hat{p}$, $\hat{\phi}$, $\hat{\sigma}$ are expanded as

$$\begin{aligned} \hat{u} &= \sum_0^N a_n T_n(\zeta), \quad \hat{v} = \sum_0^N b_n T_n(\zeta), \quad \hat{w} = \sum_0^N c_n T_n(\zeta), \\ \hat{p} &= \sum_0^N d_n T_n(\zeta), \quad \hat{\phi} = \sum_0^N e_n T_n(\zeta), \quad \hat{\sigma} = \sum_0^N f_n T_n(\zeta), \end{aligned} \tag{42}$$

where $T_n(\zeta)$ denotes the nth Chebyshev polynomial.

V. RESULTS AND DISCUSSION

This section is organized into two parts. In the first part, we consider the limiting case of an infinitely large inner radius, i.e., $a \to \infty$. We consider a two-dimensional axisymmetric system and compare our results with the previous study of Chang *et al.* [22] to examine the validity of our numerical method. The second part deals with the three-dimensional instability of the annular flow under the consideration of a finite inner radius a. The parametric studies on the stability characteristics are investigated.

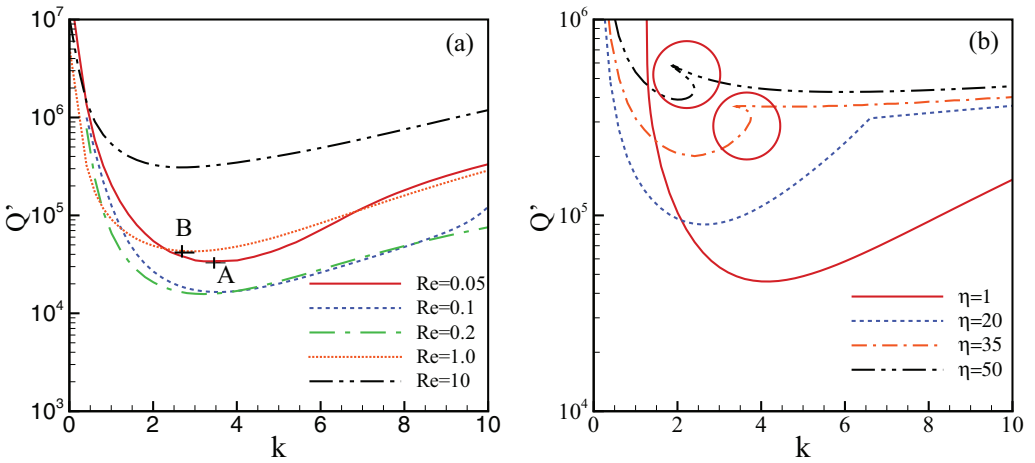

FIG. 3. (Color online) Marginal stability curves. (a) $\mathrm{Sc}_e = 1000$, $\eta = 10$. (b) $\mathrm{Re} = 1$, $\mathrm{Sc}_e = 1000$. The parameter $R_t \to \infty$.

TABLE I. The leading eigenvalues of the critical stability points A and B in Fig. 3(a).

	Re	η	k_c	Q'_c	λ
Chang *et al.* [22]	0.05	10	3.50	3.359×10^4	0–4.937i
Present work	0.05	10	3.50	3.3589×10^4	0.0000–4.9378i
Chang *et al.* [22]	1	10	2.95	4.295×10^4	0–2.850i
Present work	1	10	2.95	4.2953×10^4	0.0000–2.8503i

A. Limiting case of $a \to \infty$

This section presents the results of the eigenvalue analysis, which starts with the case of a sufficiently large radius. Hence, a small parameter can be defined as

$$\delta = \frac{b-a}{a}. \tag{43}$$

When $\delta \to 0$, the problem can be reduced to the problem studied by Chang *et al.* [22]. The governing equations for $a \to \infty$ and $n = 0$ are shown in the Appendix.

The governing system shown in the Appendix has the same form as the two-dimensional problem of Chang *et al.* when the longitudinal wave number is set to zero in Ref. [22]. The dimensionless parameter Q can be related to the Reynolds number Re and electrical Schmidt number Sc_e by

$$Q = \frac{Q'}{\mathrm{Re}^2 \mathrm{Sc}_e}, \tag{44}$$

in which $Q' = \frac{\epsilon E_0^2}{\mu K_{\mathrm{eff}}/d^2}$ represents the scaled electrical energy density.

Figure 3(a) illustrates the marginal stability curves in the Q'-k plane, which reproduces the results by Chang *et al.* [22]. The critical point (Q'_c, k_c) is compared with their results [22] in Table I. It is found that some of the results in Ref. [22] are inaccurate. When the parameter η exceeds some certain value, the marginal curve presents a bimodal structure [22], for instance, $\eta = 50$. However, this bimodal structure can be multivalued as shown in Fig. 3(b), which was overlooked by Chang *et al.* [22].

B. Finite inner radius a

This section presents the stability analysis of the annular flow system of a finite radius a. The normal mode analysis is implemented. The influence of a, Re, η, and Sc_e on the stability of the system are discussed. The parameter R_t is assumed to be infinitely large.

1. Influence of inner radius

First, we examine the influences of the inner radius a on the stability of the transverse unstable mode (the azimuthal wave number $n = 0$) by fixing the parameter $Q' = 4.2953 \times 10^4$, $\eta = 10$, $n = 0$, $k = 2.95$, $\mathrm{Re} = 1$, $\mathrm{Sc}_e = 1000$.

Figure 4(a) shows the real part of the eigenvalue, λ_r versus the disturbance wave number k and indicates that the system becomes more unstable for a larger inner radius a. The leading eigenvalue is listed in Table II, which demonstrates that the real part of growth rate becomes larger as the inner radius a increases. When a is sufficiently large, it reproduces the result showed in Sec. V A. The results indicate that, when the system is perturbed by streamwise disturbances, the system can be stabilized by reducing the inner radius a. We explain the physical mechanism here. As explained by Chang *et al.* [22], the flow instability of this system was dominated by the dielectrophoretic effect, viscosity, and ionic diffusion. When a fluid parcel with lower electrical conductivity moves outwards (in the r direction), it enters in the region of higher electrical conductivity. If the diffusion effect is not strong enough, the electrical force will drive the fluid parcel continuously. Otherwise, the ionic diffusion will remove the conductivity difference between the flowing fluid parcel and its surroundings, hence, impeding the electrohydrodynamic instability. The dielectrophoretic effect can be characterized by $\bar{\rho}_e \bar{E}_r$ [21,22]. As the charge density and electric field strength are shown in Fig. 2, it is clear that the dielectrophoretic effect becomes stronger in the region near the outer surface when the inner radius becomes larger. Therefore, the system becomes more unstable by increasing the inner radius a.

For the case of zero azimuthal wave number, $n = 0$, we define a linear wave speed c in the streamwise direction is

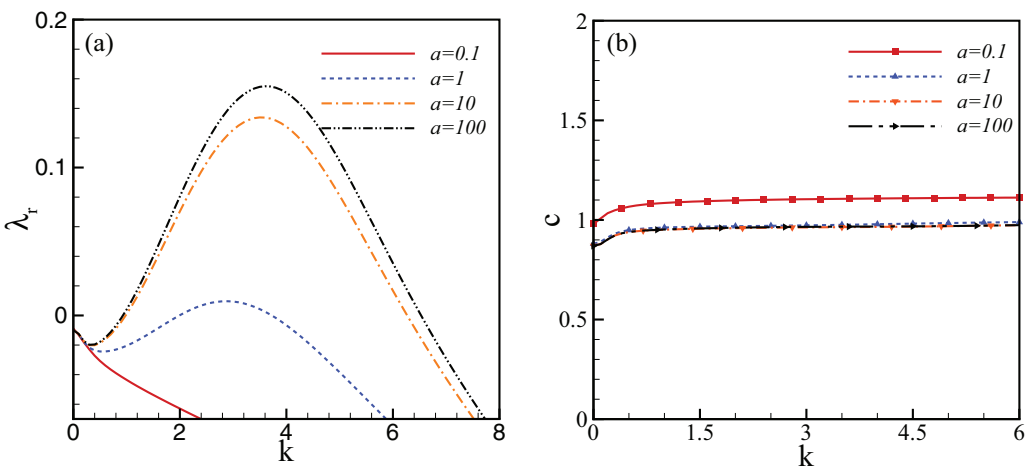

FIG. 4. (Color online) (a) Growth rate of the most unstable disturbances λ_r versus wave number k, (b) linear wave speed c versus wave number k. The dependent parameters are $\mathrm{Re} = 1$, $\mathrm{Sc}_e = 1000$, $Q' = 10^5$, $\eta = 10$, $n = 0$.

TABLE II. The first leading eigenvalues for $Q' = 4.2953 \times 10^4$, $n = 0$, $k = 2.95$, Re $= 1$, Sc$_e = 1000$, $\eta = 10$.

Inner radius	$a = 0.1$	$a = 1$	$a = 10$	$a = 100$
λ	-0.0828–$3.2580i$	-0.0479–$2.8960i$	-0.0078–$2.8509i$	-0.0008–$2.8502i$

defined as $c = -\frac{\lambda_i}{k}$. It is observed that the linear wave speed c decreases with increasing a as shown in Fig. 4(b). Additionally, c initially increases when wave number k is small, but it does not change when k is large. Apart from that, when $a \geqslant 1$, the influence of the inner radius a on the linear wave speed is not significant.

Because a Squire's transformation of this system is not possible, we need to study the influence of spanwise disturbances (disturbances in the azimuthal direction), which may cause the system to be more unstable. Figure 5 presents the marginal curves for three typical cases: $a = 0.1, 1, 10$. It is observed that the most unstable azimuthal wave number respectively is $n = 1, 5, 35$. The nonzero value of n indicates that the spanwise disturbances make the system more unstable. Here we define the lowest marginal stability curve in Figs. 5(a)–5(c) as the global marginal stability curve. Above the global marginal curve, the system is unstable. The comparison of the global marginal stability curves is shown in Fig. 5(d), which indicates that the system becomes more unstable for a larger inner radius a. It is observed that when $a = 1, 10$, the global marginal stability curve presents a bimodal structure. The bimodal structure indicates that there are two different unstable modes. Here, according to the difference in wave number, the unstable mode corresponding to a smaller wave number is defined as the long-wave unstable mode, while the mode corresponding to a larger wave number is defined as the short-wave mode. For instance, when $a = 1$ and $n = 0$ (the marginal curve presents a bimodal structure in Fig. 5(b) for $a = 1$, $n = 0$), for the long-wave unstable mode, the convection cell occupies almost the whole thickness of the fluid layer; while for the short-wave unstable mode, the convection cell is almost constrained within the inner half of the channel as shown in Fig. 6. However, the critical instability is determined by the lower branch of the bimodal structured marginal curve, indicating that the long-wave unstable mode dominates the short-wave unstable mode. Figure 5(d) shows that the frequency $-\lambda_i$ jumps down when $a = 1, 10$ showing that the unstable mode switches from the long-wave mode to the short wave mode as the wave number k increases.

When $a = 0.1$, $n = 1$, the critical value of (Q'_c, k_c) is $(6.0898 \times 10^4, 0)$, and the corresponding eigenvalue is $\lambda = 0$, indicating that the unstable mode is stationary. However,

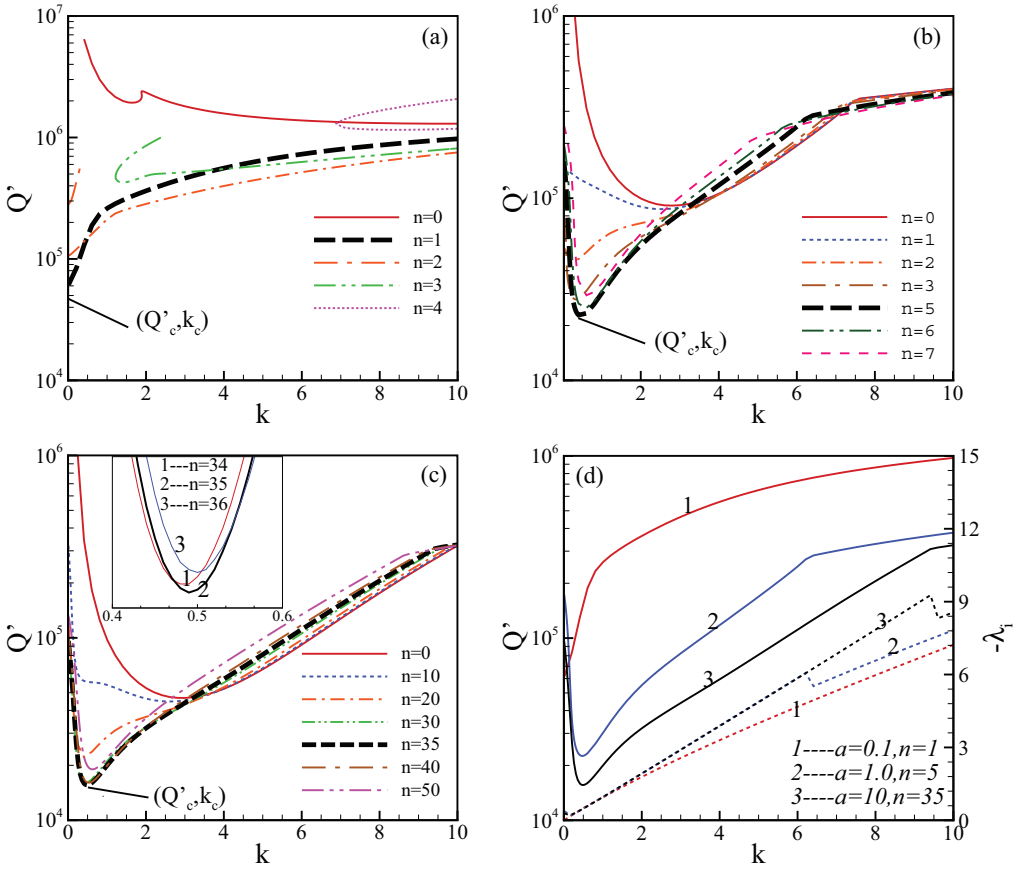

FIG. 5. (Color online) (a–c) Marginal stability curves in the $Q' - k$ plane for $a = 0.1, 1$, and 10, respectively. (d) Solid lines for the global marginal stability curves and dashed lines for the corresponding frequency $-\lambda_i$. The dependent parameters are Re $= 1$, Sc$_e = 1000$, $\eta = 10$.

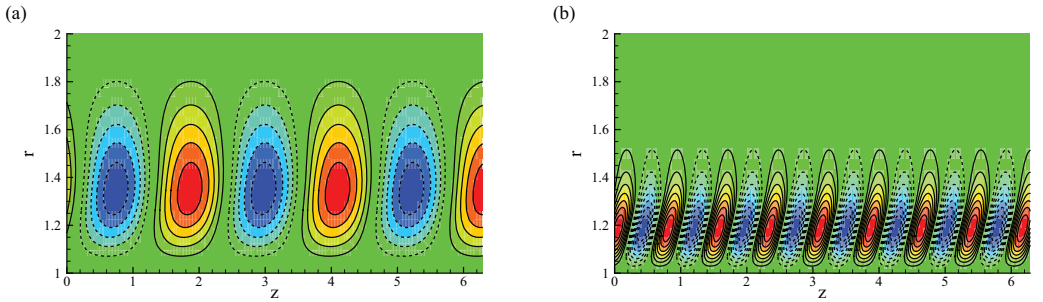

FIG. 6. (Color online) Convection cell patterns. (a) $Q' = 9.1090 \times 10^4, k = 2.81$; (b) $Q' = 36.3981 \times 10^4, k = 8.21$. The other dependent parameters are $a = 1$, Re $= 1$, Sc$_e = 1000$, $\eta = 10$, $n = 0$.

for $a = 1,10$, the critical value of (Q'_c, k_c), respectively, reads $(2.2556 \times 10^4, 0.47)$, $(1.5620 \times 10^4, 0.49)$, and the corresponding eigenvalue is $\lambda = 0 - 0.4567i$, $\lambda = 0 - 0.4748i$, respectively. The nonzero imaginary parts of eigenvalues for the two cases $a = 1,10$ indicate that the most unstable modes are given by oblique waves. In addition, we observe that the critical streamwise disturbance wave number k is much smaller than the critical azimuthal wave number n. As shown from the above discussion, the instability is triggered by the dielectrophoretic effect. According to the perturbed system, this effect is characterized by the linearized body force $\rho_e \mathbf{E}$, i.e., the radial component force $f_r = \bar{\rho}_e E'_r + \rho'_e \bar{E}_r$, the streamwise component force $f_z = \bar{\rho}_e E'_z = ik\bar{\rho}_e \hat{\phi}$, and the azimuthal component force $f_\theta = \bar{\rho}_e E'_\theta = \frac{in}{r}\bar{\rho}_e \hat{\phi}$. The magnitudes of f_z and f_θ are proportional to k and n/r, respectively. If k is much larger than n/r, the streamwise disturbances dominate the instability. Otherwise, the spanwise disturbances dominate the instability. To illustrate this, we plot the perturbed velocity field in Fig. 7. Figure 7(a) shows the velocity field (u', v'), and Fig. 7(b) presents the contour lines of the velocity component w' in the r-θ plane. The velocity field (u', v') as well as the contour lines of w' are not distorted as seen in Figs. 7(a) and 7(b). It demonstrates that the unstable mode is stationary. In Fig. 7(b) the magnitude of w' is much smaller than the magnitudes of u' and v', which demonstrates that the instability is dominated by spanwise disturbances. Figures 7(c)–7(f) show the perturbed flow fields of $a = 1,10$, in which, we observe that the velocity fields (u', v') and the contour lines of w' are distorted which implies that the unstable mode is oscillatory. In addition, in Figs. 7(d) and 7(f), the magnitude of w' is not as small as that in Fig. 7(b) indicating the most unstable mode is given by three-dimensional oblique wave.

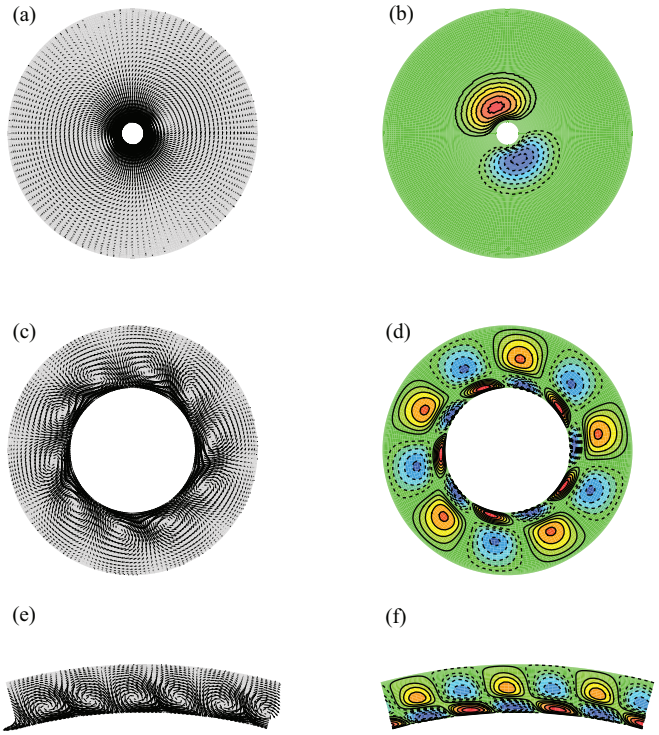

FIG. 7. (Color online) The cross section $r - \theta$ view of the flow field. (a, c, e) The velocity components of u' and v'. (b, d, f) The contour plot of velocity component w'. (e, f) $\theta \in [\frac{5\pi}{12}, \frac{7\pi}{12}]$. The dependent parameters: (a, b) $(Q'_c, k_c) = (6.0898 \times 10^4, 0)$, $a = 0.1$, $n = 1$; (c, d) $(Q'_c, k_c) = (2.2556 \times 10^4, 0.47)$, $a = 1$, $n = 5$; (e, f) $(Q'_c, k_c) = (1.5620 \times 10^4, 0.49)$, $a = 10$, $n = 35$. The other parameters are Re $= 1$, Sc$_e = 1000$, $\eta = 10$.

Figure 8 illustrates the variations of critical electric field number Q'_c, critical frequency $-\lambda_i$ and critical wave numbers n_c, k_c with the radius a. Obviously the critical electric field number Q'_c decreases with increasing a. When $a \leqslant 0.4$, the frequency $-\lambda_i$ of the most unstable mode as well as the critical wave number k_c are zero, indicating that the most unstable mode is stationary. It is discovered that the critical wave number n_c increases with increasing a, although for some cases, $a = 0.2, 0.3, 0.4$, the critical wave number is the same: $n_c = 4$. This is because the wave number n is characterized by the pairs of convection cells in the spanwise direction, which is an integer. When $a \to \infty$, the critical wave number $k \approx 0.5$, and $Q'_c \approx 1.5 \times 10^4$.

2. *Influence of electrical conductivity gradient*

In this section, the influence of the electrical conductivity gradient η on the stability is investigated. The other dimensionless parameters are held fixed. Figure 9(a) illustrates the marginal stability curves for several typical input values of electrical conductivity gradient $\eta = 0.1, 1, 10, 100$. For the selected input values of η, when the electrical conductivity gradient is small, e.g., $\eta = 0.1, 1$, increasing the value of η enhances the flow instability since the marginal curve dips lower. However, as the value of η further increases, the marginal curve rises gradually, e.g., the marginal stability curves for $\eta = 10, 100$ as shown in Fig. 9(a). The frequency

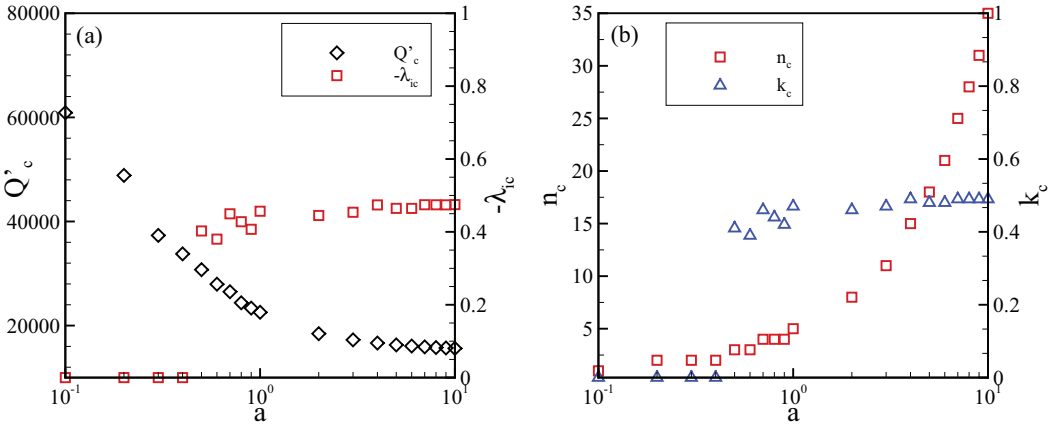

FIG. 8. (Color online) (a) The critical electric field number Q'_c and the corresponding frequency $-\lambda_i$ versus the radius a. (b) The critical wave numbers n_c and k_c versus the radius a. The other dependent parameters are Re $= 1$, Sc$_e = 1000$, $\eta = 10$.

$-\lambda_i$ versus the disturbance wave number is shown in Fig. 9(b). It shows that $-\lambda_i$ decreases as the electrical conductivity gradient increases. Particularly, it is observed that, for $\eta = 0.1, 1, 10$, the frequency $-\lambda_i$ of the critical unstable mode is not zero, which indicates the most unstable mode is oscillatory; while the critical frequency $\lambda_i = 0$ for $\eta = 100$, which indicates that the most unstable mode is stationary.

To elucidate the two different unstable modes, the perturbed flow field is plotted in Fig. 10. Figures 10(a) and 10(b) show that the flow field in the r-θ plane as well as the contour lines of w' are strongly distorted. The flow field in the r-θ plane is not distorted in Fig. 10(c). Moreover, the magnitude of w' in Fig. 10(d) in is much smaller than the magnitudes of (u', v') in Fig. 10(c). Figure 10 indicates that increasing the value of η shifts the unstable mode from the oscillatory mode to the stationary mode.

In order to have a full understanding of the influence of electrical conductivity gradient on the stability, the critical electric field number Q'_c, critical wave numbers k_c, n_c and the critical frequency $-\lambda_i$ versus the electrical conductivity η are investigated. Results are shown in Fig. 11.

Figure 11 shows that the frequency $-\lambda_i$, critical wave numbers n_c and k_c jump at $\eta \approx 17.5$, indicating that the critical unstable mode switches to the stationary mode from the oscillatory mode. The results in Fig. 11 show that the critical wave number k_c decreases gradually as the conductivity gradient increases when $\eta < 17.5$, while the wave number n_c jumps from $n = 5$ to $n = 4$ at $\eta \approx 17.5$. The decrease in k_c indicates that the spanwise disturbances become important in destabilizing the system. When the critical unstable mode switches to the stationary mode, the wave number $k_c = 0$, which indicates that the spanwise disturbances are the major causes that initiate the electroconvection in this system. Figure 11(a) shows that the critical electric field number Q'_c decreases gradually till $\eta \approx 4$, which implies that the instability of the oscillatory mode is enhanced. However, as the value of η increases further, Q'_c increases gradually and reaches a maximum, which reflects that the oscillatory mode is impeded. When the critical unstable mode switches to the stationary mode, the critical electric field number Q'_c decreases to a minimum till $\eta \approx 20$, and then it increases gradually as η increases. Such a phenomenon indicates that

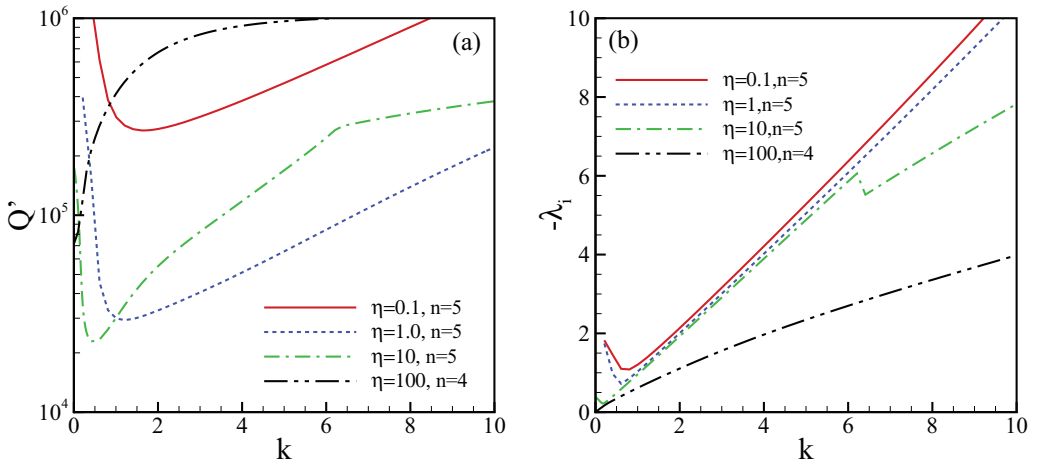

FIG. 9. (Color online) (a) Global marginal stability curves and (b) the corresponding frequency $-\lambda_i$. The other dependent parameters are $a = 1$, Re $= 1$, Sc$_e = 1000$.

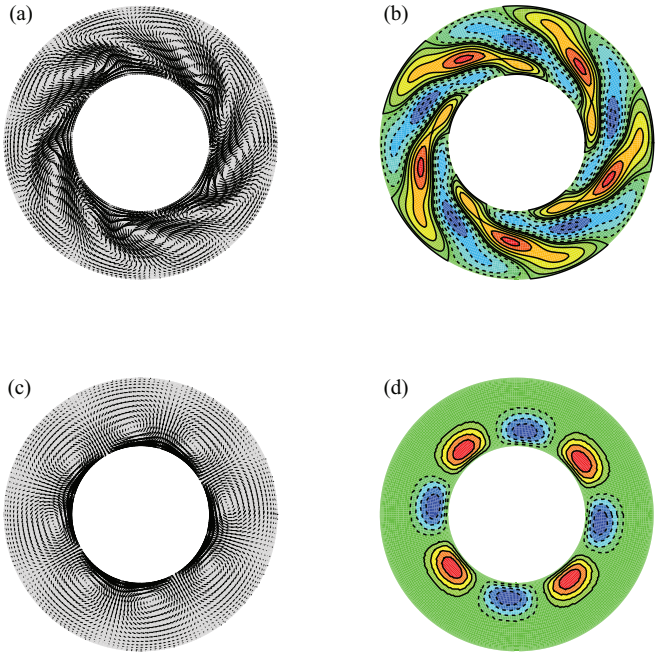

FIG. 10. (Color online) The cross section $r-\theta$ view of the flow field. (a, c) The velocity components of u' and v'. (b, d) The contour plot of velocity component w'. The dependent parameters are: (a, b) $(Q'_c,k_c) = (26.9395\times10^4,1.66)$, $n_c = 5$, $\eta = 0.1$; (c,d) $(Q'_c,k_c) = (7.1410\times10^4,0)$, $n_c = 4$, $\eta = 100$. The other parameters are $a = 1$, $\mathrm{Re} = 1$, $\mathrm{Sc}_e = 1000$.

the stationary mode can be either enhanced or impeded via increasing the conductivity gradient.

In order to understand the physical mechanism, let us consider a limiting case: $\eta \to 0$. The electrical body force term in Eq. (24) can be rewritten as

$$\mathbf{f} = Q\nabla^2\phi\nabla\phi = -\eta\rho_e Q\nabla\phi. \tag{45}$$

When $\eta \to 0$, the body force $\mathbf{f} \to 0$. Hence, no matter how large the electric field strength is, the system is always stable because the dielectrophoretic effect is absent. The mechanism can be analogous to the Rayleigh-Bénard convection. If there is no temperature gradient, the heated liquid layer should be always stable. A electrical Rayleigh number can be defined as $\mathrm{Ra}_e = Q'\eta$, which approaches zero as $\eta \to 0$. As a result, the system becomes stable when $\eta \to 0$.

If a fluid parcel moves outwards under the action of electric field, it enters the region of higher electrical conductivity. When the conductivity gradient is small (the oscillatory mode dominates the instability), the ionic diffusion effect is insignificant. As the electrical conductivity gradient is increased, the dielectrophoretic effect will be enhanced since the conductivity difference between the fluid parcel and its surroundings is increased. Consequently, the instability is enhanced. As the conductivity gradient increases, the diffusion effect becomes significant such that the conductivity difference between the fluid parcel and its surroundings will be removed due to diffusion effect. Hence, when the conductivity gradient is large, a stronger electric field is necessary to trigger the occurrence of instability. Moreover, Baygents and Baldessari [21] explained the physical electrohydrodynamic instability mechanism in a planar system by the base state profile of an electrical body force. They pointed out that the portion of fluid where the electrical body force was significant was close to the lower-conductivity boundary and became increasingly narrow as the conductivity gradient increased [21]. They suggested that the lower boundary produced a strong stabilizing effect when η was large [21]. Figure 2 suggests that the portion where the electrical body force $\bar{\rho}_e\bar{E}_r$ is significant is very narrow for a large η. It seems that the inner cylinder attracts the electrical charge into the thin boundary layer, beyond which there are very few electrical charges. As discussed in Sec. VB1, the convection is initiated by the body force $(f_r,f_\theta,f_z) = (\bar{\rho}_e E'_r + \rho'_e\bar{E}_r,\bar{\rho}_e E'_\theta,\bar{\rho}_e E'_z)$. Outside the boundary layer, the charge density $\bar{\rho}_e \approx 0$ and $\bar{E}_r \approx 0$ when η is large. Hence, the body force outside the boundary layer is too small to initiate convection in the system. Note that the electrical force is multiplied by the dimensionless parameter Q'. Thus, a higher value of Q' is necessary to trigger the instability of this system.

When the instability is dominated by the stationary mode, the physical mechanism is similar to the oscillatory mode. This is very different from the classical Rayleigh-Bénard convection, in which the larger temperature gradient is the more unstable system.

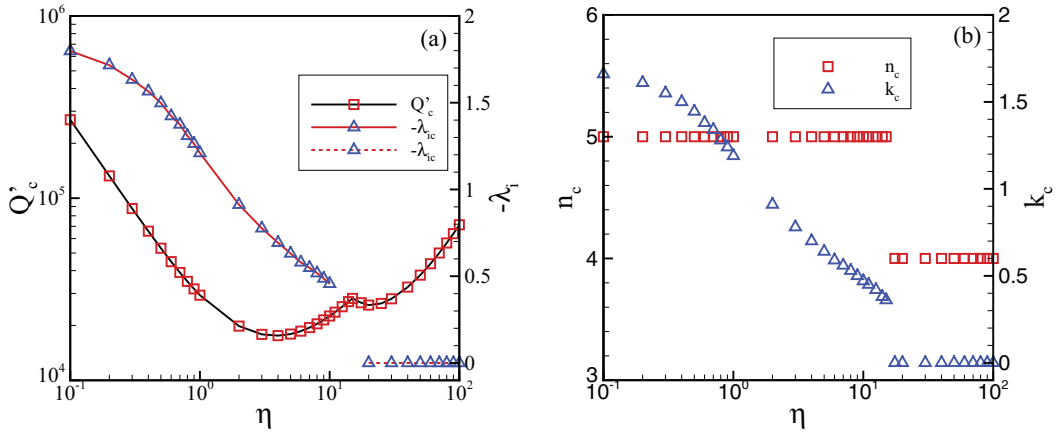

FIG. 11. (Color online) (a) The critical electric field number Q'_c and the corresponding frequency $-\lambda_i$ versus η. (b) The critical wave numbers n_c and k_c versus η. The other dependent parameters are $a = 1$, $\mathrm{Re} = 1$, $\mathrm{Sc}_e = 1000$.

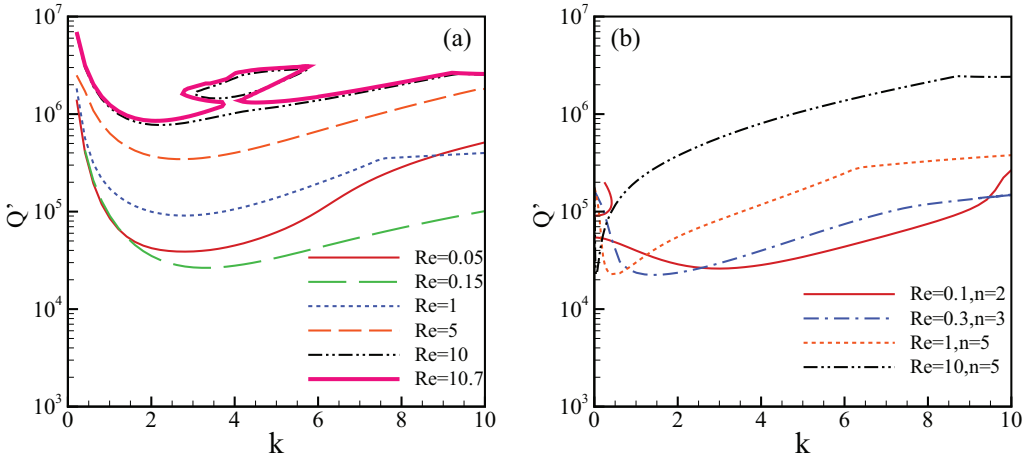

FIG. 12. (Color online) (a) Marginal stability curves of the transverse unstable mode, $n = 0$. (b) The global marginal stability curve. The other dependent parameters are $a = 1$, $\mathrm{Sc}_e = 1000$, $\eta = 10$.

3. *Influence of Reynolds number*

In this section the influence of the Reynolds number on the stability of this system is discussed by fixing the other dimensionless parameters. First, in Fig. 12(a) we show the influence of Re on the stability of transverse unstable mode, i.e., $n = 0$. When Re is small, the marginal stability curve dips lower gradually till about $\mathrm{Re} \approx 0.15$, then it rises rapidly. Results in Fig. 12(a) indicate that, when Re is small, the instability is enhanced by the shear flow, while when Re is large, the shear flow impedes the instability. The physical mechanism is explained here. When the Reynolds number is small, with increasing Re, the electrohydrodynamic motion will be enhanced. Therefore, the system will be more unstable when the Reynolds number increases. However, as the Reynolds number is increased further, the viscous shear effect and the diffusive effect become significant. Due to the advection of electrical conductivity, a conspicuous enhancement of diffusive effect would be caused by increasing the Reynolds number. Furthermore, the viscous stress is a factor that dissipates energy of the system, which plays a

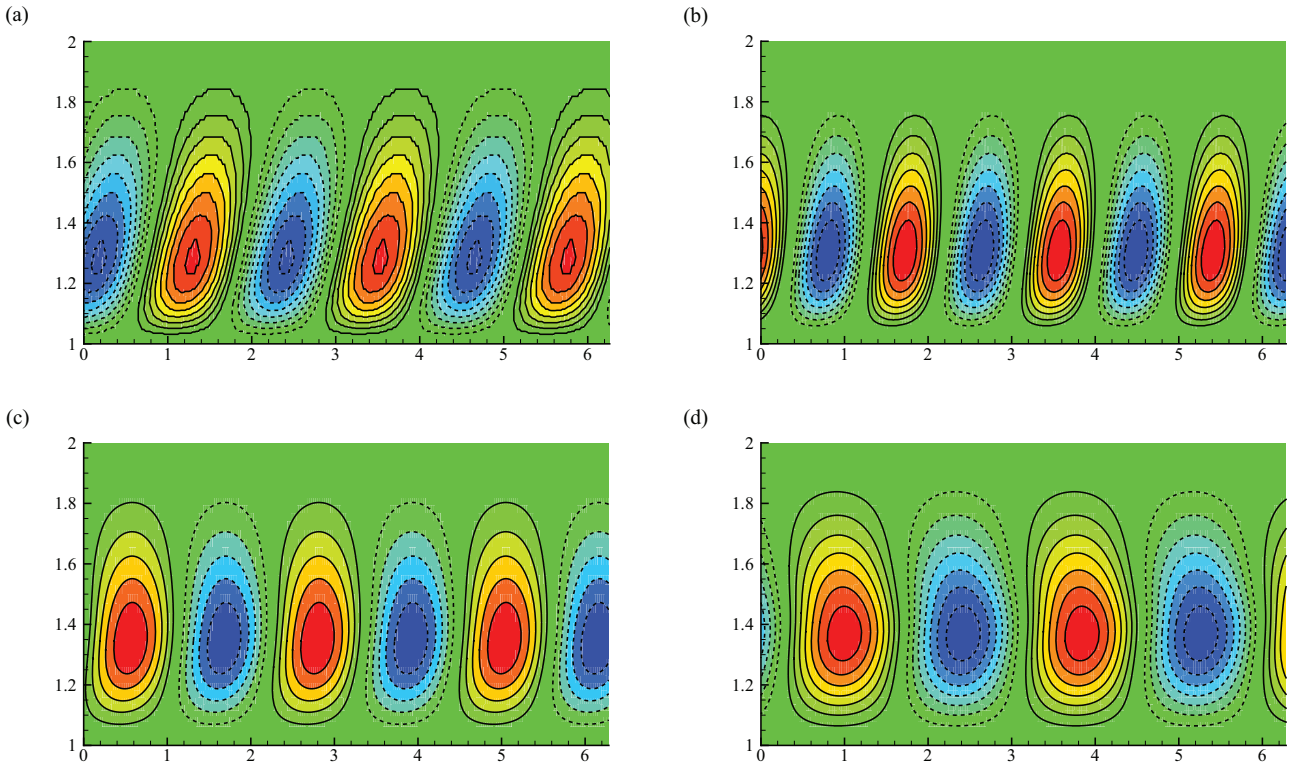

FIG. 13. (Color online) Convection cell patterns. (a) $\mathrm{Re} = 0.05$, $Q' = 3.8855 \times 10^4$, $k = 2.81$; (b) $\mathrm{Re} = 0.1$, $Q' = 2.6883 \times 10^4$, $k = 3.41$; (c) $\mathrm{Re} = 1$, $Q' = 9.1090 \times 10^4$, $k = 2.81$; (d) $\mathrm{Re} = 10$, $Q' = 77.2105 \times 10^4$, $k = 2.21$. The other dependent parameters are $a = 1$, $\mathrm{Sc}_e = 1000$, $\eta = 10$.

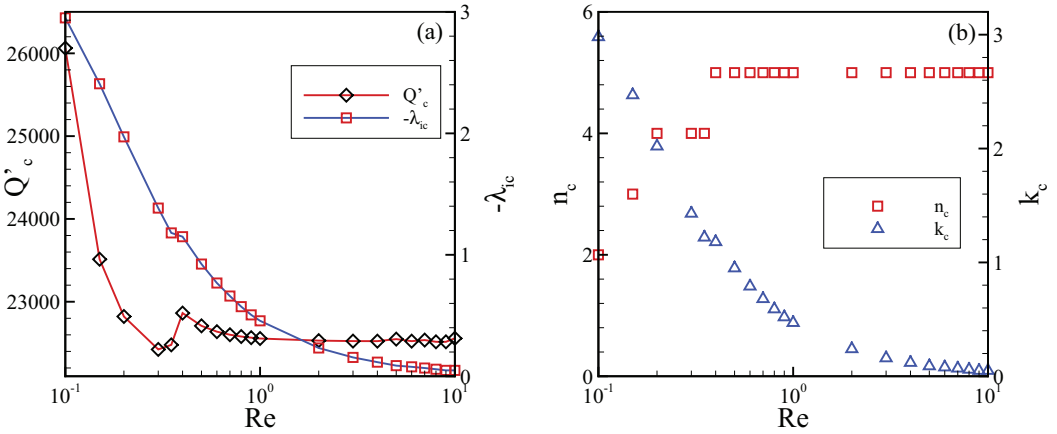

FIG. 14. (Color online) (a) The critical electric field number Q'_c and the corresponding frequency $-\lambda_i$ versus Re. (b) The critical wave numbers n_c and k_c versus Re. The other dependent parameters are $a = 1$, $\mathrm{Sc}_e = 1000$, $\eta = 10$.

stabilizing role in this system and will also be enhanced as Re increases. Once the diffusive effect and viscous dissipation effect are strong, the marginal stability curve will rise when the Reynolds number is increased further. An interesting phenomenon observed is that there may exist a stable looped region lying in the above of the marginal stability curve when Re is increased, for instance, $\mathrm{Re} = 10$. This phenomenon is caused by the interactions between the dielectrophoretic effect, viscous effect, and ionic diffusive effect. The stable looped region will vanish when Re increases further. To illustrate the above discussion, we plot the convection cell patterns of four typical cases at their corresponding critical state with $\mathrm{Re} = 0.05, 0.1, 1, 10$ in Fig. 13. As seen in Fig. 13(a), the transverse mode appears to be inclined traveling wave in the streamwise direction. When Re is increased to 0.1, convection near the outer electrode becomes weaker because the diffusive effect near the outer electrode is enhanced by the shear flow. The inclined angle is also reduced if compared with the case $\mathrm{Re} = 0.05$. As Re increases further, the inclined angle reduces continuously. When $\mathrm{Re} = 10$, the convection cell appears to be distorted, which is caused by the imposed shear flow. However, the transverse mode may not be critical because the spanwise disturbances may make the system to be more unstable.

Figure 12(b) presents the global marginal stability curve. Comparing Figs. 12(a) and 12(b), we observe that the system is more unstable when it is perturbed by three-dimensional disturbances. Moreover, it is observed that the critical point (Q'_c, k_c) moves leftward as the Reynolds number increases. In order to explain the influences of Reynolds number on the stability of the three-dimensional problem, the critical electric field number Q'_c, the critical frequency $-\lambda_{ic}$, the critical wave number n_c and k_c are investigated. The results are shown in Fig. 14.

In Fig. 14(a), we observe that the critical electric field number Q'_c decreases with Re gradually until $\mathrm{Re} \approx 0.3$, then it increases till $\mathrm{Re} \approx 0.4$. After that, Q'_c decreases gradually, and when $\mathrm{Re} \geqslant 1$, the influence of Reynolds number on Q'_c is not significant. The critical frequency decreases as Re increases and $\lambda_i \approx 0$ at $\mathrm{Re} = 10$. In Fig. 14(b), when $\mathrm{Re} < 0.3$, the critical wave number k_c decreases, while n_c increases. The instability is triggered by the dielectrophoretic force $\mathbf{f}$. When $k_c > n_c/r$, f_z dominates f_θ, i.e., convection in the r-z plane is stronger than that in the r-θ plane. As we have discussed above, a slightly increasing in the Reynolds number from zero will enhance the dielectrophoretic effect. Thus, Q'_c decreases with increasing the Reynolds number

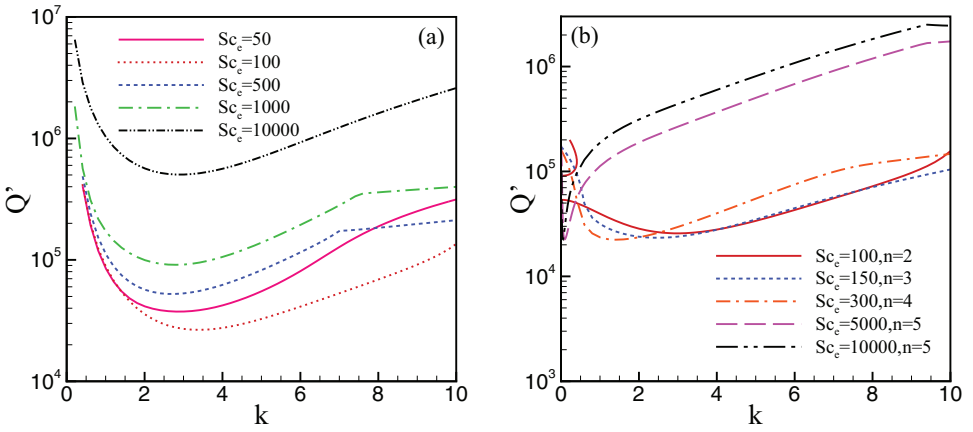

FIG. 15. (Color online) (a) Marginal stability curves of the transverse unstable mode, $n = 0$. (b) The global marginal stability curve. The other dependent parameters are $a = 1$, $\mathrm{Re} = 1$, $\eta = 10$.

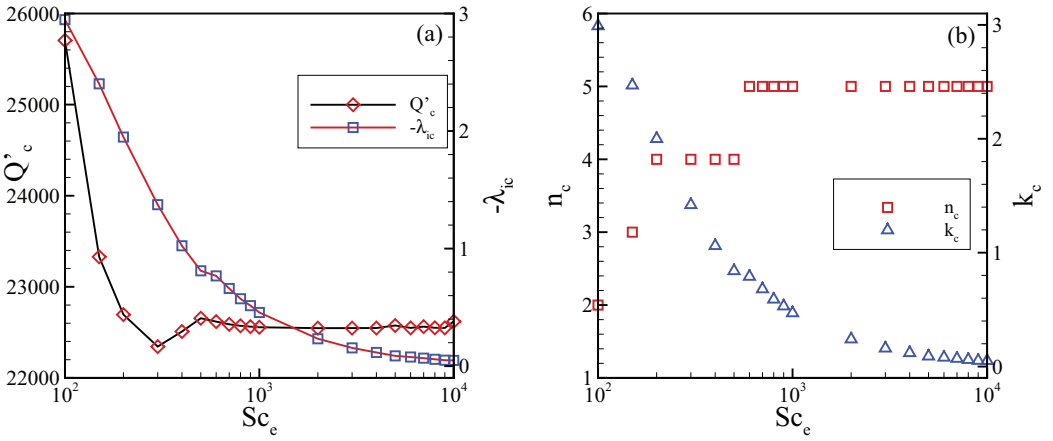

FIG. 16. (Color online) (a) The critical electric field number Q'_c and the corresponding frequency $-\lambda_i$ versus Sc_e. (b) The critical wave numbers n_c and k_c versus Sc_e. The other dependent parameters are $a = 1$, $\mathrm{Re} = 1$, $\eta = 10$.

until it reaches a minimum value. As the Reynolds number is increased further, the convection in the r-z plane will be impeded due to the enhancement of diffusive effect, hence Q'_c increases. After Q'_c reaches a maximum value, Q'_c gradually decreases as the Reynolds number increases further till about $\mathrm{Re} \approx 1$, because the dielectrophoretic effect in θ direction is enhanced. When $\mathrm{Re} > 1$, Q'_c is almost independent of the shear flow. It is evident in Fig. 14(b) that n_c/r ($r \in [1,2]$) is much larger than k_c when $\mathrm{Re} > 1$, which indicates the streamwise wavelength of the disturbance is much longer than its spanwise component, and the convection in the r-θ plane is much stronger than that in the r-z plane. When $\mathrm{Re} > 1$, although the spanwise disturbance becomes the major cause that destabilizes the system, the long-wave streamwise disturbance would make the system to be more unstable.

4. *Influence of electric Schmidt number*

The influence of the electrical Schmidt number Sc_e is investigated in this section. Its influence on the marginal stability curve of transverse mode is illustrated in Fig. 15(a). The marginal stability curve dips lower as Sc_e increases till $\mathrm{Sc}_e \approx 150$. It then rises rapidly as Sc_e increases. Recall the definition of this parameter: $\mathrm{Sc}_e = \frac{\nu}{K_{\mathrm{eff}}}$. The value of Sc_e can be increased by reducing K_{eff}. Hence, the ionic diffusive effect becomes smaller as Sc_e increases. Therefore, the dielectrophorectic effect is enhanced as Sc_e increases (K_{eff} decreases), and the system becomes more unstable. However, on the other hand, for a large Sc_e, the definition of Sc_e tells us that the viscous effect dominates the diffusion effect, and the viscous effect becomes significant with increasing Sc_e. Since the viscous effect plays a stabilizing role in the system, the fluid layer will be stabilized as Sc_e increases further.

The global marginal stability curve for the three-dimensional problem is shown in Fig. 15(b). Clearly, with increasing the value of Sc_e, the critical wave number k_c decreases, which indicates that the streamwise component of the wavelength becomes longer. In order to understand the influence of electrical Schmidt number on the three-dimensional stability, we plot the critical electric field number Q'_c and the critical frequency $-\lambda_{ic}$ in Fig. 16(a). Note that the critical wave number $n_c \neq 0$ and critical frequency $\lambda_{ic} \neq 0$, which indicates that the critical unstable mode was given by three-dimensional oblique waves. The critical frequency $-\lambda_{ic}$ approaches zero when Sc_e is very large. Additionally, it is observed that Q'_c decreases with increasing the value of Sc_e till $\mathrm{Sc}_e \approx 300$, then it increases with increasing Sc_e till $\mathrm{Sc}_e \approx 500$. As Sc_e increases further, Q_c decreases slightly, and then Q'_c seems to be independent of Sc_e. It was reported by Chang *et al.* [22] that the influence of Sc_e on the longitudinal unstable mode in a planar system was insignificant when $\mathrm{Sc}_e \geqslant 10^3$. Similarly, in this core-annular system, the Q'_c almost does not vary with Sc_e when $\mathrm{Sc}_e \geqslant 10^3$ because the the spanwise disturbance is the major cause of the flow instability.

VI. CONCLUSION

In this paper, the three-dimensional linear instability of an annular liquid layer with radial electrical conductivity gradient in a radial electric field was investigated. A weak shear flow arose from an axial constant pressure gradient. The critical unstable mode was found to be either oscillatory or stationary, which was dependent on these dimensionless parameters: the dimensionless inner radius a, the electrical conductivity gradient η, the Reynolds number Re, and the electrical Schmidt number Sc_e.

To discuss the influence of the radius a on the instability, the other dimensionless parameters were fixed: $\eta = 10$, $\mathrm{Re} = 1$, and $\mathrm{Sc}_e = 10^3$. When the dimensionless radius $a < 0.4$, the major cause of instability was the azimuthal disturbance, and the critical unstable mode was stationary. When $a > 0.4$, the critical unstable mode was given by the there-dimensional oblique waves. Notably, the system became more unstable as the radius a increased.

The influence of the conductivity gradient η on the instability was examined. The other dimensionless parameters were fixed at $a = 1$, $\mathrm{Re} = 1$, and $\mathrm{Sc}_e = 10^3$. When the conductivity gradient was small, the critical unstable mode was given by the three-dimensional oblique wave. As the conductivity gradient increased, the system became more unstable because the dielectrophoretic effect was enhanced. However, as the conductivity gradient increased further, the instability of the system was suppressed due to the enhancement of ionic diffusion and the stationary mode became critical when $\eta \gtrapprox 17.5$.

In order to understand the influence of the imposed shear flow, the Reynolds number was varied while the other parameters were fixed: $a = 1, \eta = 10, \mathrm{Sc}_e = 10^3$. It was found that, the system became more unstable when Re was slightly increased from zero. When $\mathrm{Re} > 1$, the critical electrical number $Q_c{}'$ seemed to be independent of Re. The critical unstable modes were three-dimensional oblique waves.

In the last part of Sec. V, the effect of electrical Schmidt number Sc_e on the flow instability was investigated. The other parameters were held fixed at $a = 1$, $\eta = 10$, $\mathrm{Re} = 1$. The three-dimensional system may either be more unstable or more stable as Sc_e increased. When $\mathrm{Sc}_e > 10^3$, the critical electrical number $Q_c{}'$ seemed not to be influenced by Sc_e.

ACKNOWLEDGMENTS

The authors acknowledge support from the Singapore Ministry of Education Academic Research Fund Tier 2 research grant MOE2011-T2-1-036. The authors acknowledge the referees for their many helpful comments. Ding Zijing thanks Sabnavis Bindumadhav for his suggestions.

APPENDIX

Here we show the fully linearized equations of the system:

$$\frac{\partial u'}{\partial r} + \frac{u'}{r} + \frac{1}{r}\frac{\partial v'}{\partial \theta} + \frac{\partial w'}{\partial z} = 0, \tag{A1}$$

$$\frac{\partial u'}{\partial t} + \bar{w}\frac{\partial u'}{\partial z} = -\frac{\partial p'}{\partial r} + \frac{1}{\mathrm{Re}}\left(\nabla^2 u' - \frac{u'}{r^2} - \frac{2}{r^2}\frac{\partial v'}{\partial \theta}\right) + Q\left(\nabla^2\bar{\phi}\frac{\partial \phi'}{\partial r} + \frac{\partial \bar{\phi}}{\partial r}\nabla^2\phi'\right), \tag{A2}$$

$$\frac{\partial v'}{\partial t} + \bar{w}\frac{\partial v'}{\partial z} = -\frac{1}{r}\frac{\partial p'}{\partial \theta} + \frac{1}{\mathrm{Re}}\left(\nabla^2 v' - \frac{v'}{r^2} + \frac{2}{r^2}\frac{\partial u'}{\partial \theta}\right) + \frac{Q\nabla^2\bar{\phi}}{r}\frac{\partial \phi'}{\partial \theta}, \tag{A3}$$

$$\frac{\partial w'}{\partial t} + \bar{w}\frac{\partial w'}{\partial z} = -\frac{d\bar{w}}{dr}u' - \frac{\partial p'}{\partial z} + \frac{1}{\mathrm{Re}}\nabla^2 w' + Q\nabla^2\bar{\phi}\frac{\partial \phi'}{\partial z}, \tag{A4}$$

$$\frac{\partial(\nabla^2\phi')}{\partial t} + \bar{w}\frac{\partial(\nabla^2\phi')}{\partial z} = -\frac{d(\nabla^2\bar{\phi})}{dr}u' - R_t\left[(1+\eta\bar{\sigma})\nabla^2\phi' + \eta\left(\nabla^2\bar{\phi}\sigma' + \frac{d\bar{\phi}}{dr}\frac{\partial \sigma'}{\partial r} + \frac{d\bar{\sigma}}{dr}\frac{\partial \phi'}{\partial r}\right)\right], \tag{A5}$$

$$\frac{\partial \sigma'}{\partial t} + \bar{w}\frac{\partial \sigma'}{\partial z} = -\frac{d\bar{\sigma}}{dr}u' + \frac{1}{\mathrm{ReSc}_e}\nabla^2\sigma', \tag{A6}$$

where $\nabla^2 = \frac{\partial^2}{\partial r^2} + \frac{1}{r}\frac{\partial}{\partial r} + \frac{1}{r^2}\frac{\partial^2}{\partial \theta^2} + \frac{\partial^2}{\partial z^2}$ and noting that $\nabla^2\bar{\phi} = -\eta\bar{\rho}_e$, $\frac{\partial \bar{\phi}}{\partial r} = -\bar{E}_r$.

When the radius $a \to \infty$, the base state reduces to the problem studied by Chang *et al.* [22]:

$$\bar{w}(x) = 4(x - x^2), \tag{A7}$$

$$\bar{\sigma} = x, \tag{A8}$$

$$\bar{E}_r = \frac{1}{\eta x + 1}, \tag{A9}$$

$$\bar{\phi} = -\frac{1}{\eta}\ln(\eta x + 1), \tag{A10}$$

$$\bar{\rho}_e = -\frac{1}{(\eta x + 1)^2}, \tag{A11}$$

where $x = r - a$ represents the wall-normal direction.

When the azimuthal wave number $n = 0$ and $a \to \infty$, the eigenvalue problem reduces to

$$\mathtt{D}\hat{u} + ik\hat{w} = 0, \tag{A12}$$

$$\lambda\hat{u} + ik\bar{w}\hat{u} = -\mathtt{D}\hat{p} + \frac{1}{\mathrm{Re}}\mathscr{L}\hat{u} + Q[\mathtt{D}^2\bar{\phi}\mathtt{D}\hat{\phi} + \mathtt{D}\bar{\phi}\mathscr{L}\hat{\phi}], \tag{A13}$$

$$\lambda\hat{w} + ik\bar{w}\hat{w} = -\mathtt{D}\bar{w}\hat{u} - ik\hat{p} + \frac{1}{\mathrm{Re}}\mathscr{L}\hat{w} + ikQ\mathtt{D}^2\bar{\phi}\hat{\phi}, \tag{A14}$$

$$\lambda\mathscr{L}\hat{\phi} + ik\bar{w}\mathscr{L}\hat{\phi} = -\mathtt{D}^3\bar{\phi}\hat{u} - R_t[(1+\eta\bar{\sigma})\mathscr{L}\hat{\phi} + \eta(\mathtt{D}^2\bar{\phi}\hat{\sigma} + \mathtt{D}\bar{\phi}\mathtt{D}\hat{\sigma} + \mathtt{D}\bar{\sigma}\mathtt{D}\hat{\phi})], \tag{A15}$$

$$\lambda\hat{\sigma} + ik\bar{w}\hat{\sigma} = -\mathtt{D}\bar{\sigma}\hat{u} + \frac{1}{\mathrm{ReSc}_e}\mathscr{L}\hat{\sigma}, \tag{A16}$$

where $\mathscr{L} = \mathtt{D}^2 - k^2$, $\mathtt{D} = \frac{d}{dx}$.

The Eqs. (A12)–(A16) are solved with the boundary conditions at $x = 0, 1$:

$$\hat{u} = \hat{w} = \hat{\sigma} = \mathtt{D}\hat{\phi} = 0. \tag{A17}$$

The above system is identical to the two-dimensional problem studied by Chang *et al.* [22].

[1] R. Magarvey and L. Outhouse, J. Fluid Mech. **13**, 151 (1962).
[2] S. Niamlang and A. Sirivat, Drug Delivery **16**, 378 (2010).
[3] H. Lin, Mech. Res. Comm. **36**, 33 (2009).
[4] J. Melcher and W. Schwartz, Phys. Fluids **11**, 2604 (1968).
[5] J. Melcher and C. Smith, Phys. Fluids **12**, 778 (1969).
[6] D. A. Saville, Annu. Rev. Fluids **29**, 27 (1997).
[7] O. Ozen, N. Aubry, D. T. Papageorgiou, and P. G. Petropoulos, Phys. Rev. Lett. **96**, 144501 (2006).
[8] F. Li, O. Ozen, N. Aubry, D. T. Papageorgiou, and P. G. Petropoulos, J. Fluid Mech. **583**, 347 (2007).
[9] H. Lin, B. D. Storey, M. H. Oddy, C. H. Chen, and J. G. Santiago, Phys. Fluids **16**, 1922 (2004).
[10] J. Melcher and M. Firebaugh, Phys. Fluids **10**, 1178 (1967).

[11] J. J. Santos and B. D. Storey, Phys. Rev. E **78**, 046316 (2008).
[12] G. I. Taylor, Proc. R. Soc. Lond. A **291**, 159 (1966).
[13] C. L. Burcham and D. A. Saville, J. Fluid Mech. **452**, 163 (2002).
[14] J. M. López-Herrera, P. Riesco-Chueca, and A. M. Gañón-Calvo, Phys. Fluids **17**, 034106 (2005).
[15] Q. Wang, Phys. Fluids **24**, 102102 (2012).
[16] Z. Ding, T. N. Wong, and H. Li, Phys. Fluids **25**, 124103 (2013).
[17] A. W. Wray, O. Matar, and D. T. Papageorgiou, IMA J. Appl. Math. **77**, 430 (2012).
[18] A. Wray, D. T. Papageorgiou, and O. Matar, J. Fluid Mech. **735**, 427 (2013).
[19] J. F. Hoburg and J. R. Melcher, Phys. Fluids **20**, 903 (1977).
[20] W. Thormann, R. A. Mosher, and M. Bier, J. Chromatography **351**, 17 (1986).
[21] J. C. Baygents and F. Baldessari, Phys. Fluids **10**, 301 (1998).
[22] M. H. Chang, A. C. Ruo, and F. Chen, J. Fluid Mech. **634**, 191 (2009).
[23] P. Carriere and P. Monkewitz, J. Fluid Mech. **384**, 243 (1999).
[24] R. Clever and F. Busse, J. Fluid Mech. **234**, 511 (1999).
[25] A. C. Ruo, M. H. Chang, and F. Chen, Phys. Fluids **22**, 024102 (2010).
[26] E. Georgiou, D. T. Papageorriou, C. Maldarelli, and D. S. Rumschitzki, J. Fluid Mech. **226**, 149 (1991).
[27] D. Conroy, O. Matar, R. Craster, and D. Papageorgiou, J. Fluid Mech. **656**, 481 (2010).
[28] D. Conroy, O. Matar, R. Craster, and D. Papageorgiou, Phys. Fluids **23**, 022103 (2011).
[29] D. Conroy, O. Matar, R. Craster, and D. Papageorgiou, J. Fluid Mech. **701**, 171 (2012).
[30] I. S. Shivakumaraa, J. Leeb, K. Vajraveluc, and M. Akkanagammaa, Int. J. Heat Mass Trans. **55**, 2984 (2012).
[31] H. N. Yoshikawa, M. Tadie Fogaing, O. Crumeyrolle, and I. Mutabazi, Phys. Rev. E **87**, 043003 (2013).
[32] M. Takashima, Q. J. Mech. Appl. Math. **33**, 93 (1980).
[33] P. J. Stiles and M. Kagan, Physica A **197**, 583 (1993).
[34] H. N. Yoshikawa, O. Crumeyrolle, and I. Mutabazi, Phys. Fluids **25**, 024106 (2013).
[35] J. Melcher, *Continuum Electromechanics* (MIT Press, Cambridge, MA, 1981).